euronoise

Acoustic pulse attenuation and transmission in rigid porous media: Experimental investigation and numerical simulations

Diego Turo and Olga Umnova

University of Salford, Acoustics Research Centre, Newton Building, M5 4WT Salford, UK
d.turo@pgr.salford.ac.uk

This paper presents investigations of the acoustic pulse propagation in rigid porous media. Transmission measurements of acoustic pulses through granular materials were performed using a specially constructed vertically installed standing wave tube. First, material microstructure and pulse durations were adapted to investigate the influence of viscous and inertial effects on pulse propagation. Semi-empirical time domain equations employing two viscous and two thermal relaxation times were solved numerically to predict the impulse response of the granular materials.
Comparison between the model predictions and data were undertaken. Accuracy and computational time required for the numerical simulations have been estimated and compared with that required for a simpler model implementation.

1 Introduction

Most theories of wave interaction with porous materials are formulated in the frequency domain, but interest in time domain models is growing due to potential applications such as finite-difference time-domain (FDTD) simulation of outdoor sound propagation phenomena in the presence of an absorbing surface. However, model and numerical procedures for realistically incorporating interactions with porous ground surfaces remains problematic Ground interaction could be incorporated into an FDTD calculation in two ways: developing a time domain counterpart to a frequency domain impedance boundary condition, [1, 2] or explicitly calculating the sound wave propagation into the porous medium [3, 4, 5].
For the last approach the time domain analogue of the Zwikker and Kosten model [6] can be used but it is not clear whether these simple time-domain equations are generally realistic for porous granular materials. On the other hand, frequency domain microstructural models as the ones developed by Attenborough [7] are not analytically transferable into the time domain. Wilson *et al*. employed an explicit calculation method adopting time domain equations based on modelling viscous and thermal diffusion in porous material as relaxation processes [8, 9]. However this model does not allow matching physically correct low and high frequency limits [10] with a single pair of viscous and thermal relaxation times. In this work, FDTD simulations based on the semi-empirical time domain model formulated in [11] are presented. The model, originally formulated in frequency domain, can be seen as a generalisation of [9] and requires two viscous relaxation times and two thermal relaxation times to match correct low and high frequency limits. It provides two sets of time domain equations depending on the values of viscous and thermal shape factors, M and M' respectively.
Particular attention is given to granular materials and their acoustic pulse response. A vertically installed impedance tube has been built which is specially designed for transmission measurements in time domain. The pulse response of different granular materials has been investigated for long as well as short pulses and the results of FDTD simulations are compared with data.
The paper is organised as follows. In section 2, frequency domain impedance measurement results on packings of spherical particles are presented. These measurements were necessary to perform in order to validate the frequency-domain semi-empirical model and the chosen set of material parameters. In section 3 the numerical methods used for the solution of the time-domain equations are described. Section 4 contains description of the experimental set-up used for the pulse transmission measurements and comparisons between the data and the model predictions. Main findings and future work are summarised in the conclusion.

2 Model validation in frequency domain

Reflection and absorption coefficients of the packings of spherical particles have been measured for comparison with the model predictions. In order to make measurements on granular materials a vertical impedance tube was built. This tube has a diameter of 0.104 m and a variable length, depending on the chosen set up, of 0.94 and 2.10 meters.
According to the British Standards [12, 13], with a microphone spacing of 0.095 m, this tube allowed measurements in the frequency range between 200 Hz and 1400 Hz. The set up is shown in Fig. 1.
The transfer function method was used to evaluate the reflection and absorption coefficients.
In order to determine the reflection coefficient R, the following relationship was used:

$$R = \frac{H_{12} - \exp\left[-jk\left(z_1 - z_2\right)\right]}{\exp\left[jk\left(z_1 - z_2\right)\right] - H_{12}} \exp\left(j2kz_2\right) \quad (1)$$

where k is the wavenumber, H_{12} is the transfer function between the two microphones, z_1 and z_2 are the distances of microphone 1 and microphone 2 from the surface of the sample respectively. The absorption coefficient A was determined using the following expression

$$A = 1 - \left|R\right|^2 \quad (2)$$

The samples were chosen to be the closest approximation to a rigid packing of spheres. Marbles, two types of lead shot and sand were tested for this work.

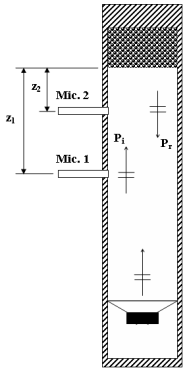

Fig. 1 Impedance tube set-up.

To compare the data with the model predictions, the knowledge of the following six material parameters is necessary: tortuosity α_∞, porosity ϕ, static flow resistivity σ, viscous characteristic length Λ, thermal (or entropic) characteristic length Λ_e and thermal permeability k'. The only measured parameter was the porosity, whereas the other parameters were evaluated using the cell model [14]. In agreement with other authors [15], a value of viscous shape factor *M* greater then 1 was found for the packings of spheres. Parameters of the samples are summarised in Table 1. Thanks to the correlation between pore size and critical angular frequency

$$\omega_c = \frac{\eta\phi}{\rho_0\alpha_\infty k_0} \tag{3}$$

investigation in the whole range of frequencies was made possible by changing the size of the spheres. Investigations at the low frequencies $\omega < \omega_c$, where viscous effects dominate, was possible using small particles (sand). Higher frequency range $\omega > \omega_c$, where inertial effects are stronger, has been investigated using bigger spheres (marbles and lead shot). A good agreement with the frequency domain data and the model formulated in [10] for the case M>1, M'>1 has been found which is demonstrated in Fig. 2. The model utilises the following equations for complex density and complex compressibility functions

$$\alpha_1(\omega) = \frac{\alpha_\infty}{1-\frac{1}{2}\left(\frac{1}{\sqrt{1-i\omega\tau_1}}+\frac{1}{\sqrt{1-i\omega\tau_2}}\right)} \tag{4}$$

$$C_1(\omega) = 1+\frac{\gamma-1}{2}\left(\frac{1}{\sqrt{1-i\omega\tau_{e,1}}}+\frac{1}{\sqrt{1-i\omega\tau_{e,2}}}\right) \tag{5}$$

where two pairs of viscous $\tau_{1,2}$ and thermal $\tau_{e,1,2}$ relaxation times are determined as

$$\tau_{1,2} = \frac{2\alpha_\infty\rho_0}{\sigma\varphi}\left(1\pm\sqrt{1-\left(\frac{1+\sqrt{8M+1}}{4M}\right)^2}\right) \tag{6}$$

$$\tau_{e,1,2} = \frac{2k'N_{pr}}{v\phi M'}\left(1\pm\sqrt{1-\frac{\sqrt{8M'+1}-1}{2M'}}\right)^{-2} \tag{7}$$

3 Semi-empirical time domain model and its numerical implementation

Inverse Fourier transformation of momentum conservation and continuity equations with functions Eq.(4) and Eq.(5) leads to the following set of time-domain equations:

$$\partial_t V = -b\partial_x P + \frac{b}{2\sqrt{\pi}}\int_{-\infty}^{t}\frac{\partial_x P(t')}{\sqrt{t-t'}}\sum_{m=1}^{2}\frac{\exp\left(-\frac{t-t'}{\tau_m}\right)}{\sqrt{\tau_m}} \tag{8}$$

$$\partial_t P + \frac{\gamma-1}{2\sqrt{\pi}}\int_{-\infty}^{t}\frac{\partial_{t'}P(t')}{\sqrt{t-t'}}\sum_{m=1}^{2}\frac{\exp\left(-\frac{t-t'}{\tau_{e,m}}\right)}{\sqrt{\tau_{e,m}}}dt' = -K\partial_x V \tag{9}$$

where $b = \frac{\varphi}{\alpha_\infty\rho_0}$, $K = \frac{\gamma P_0}{\phi}$. For further convenience the equations are formulated for pressure *P* and the volume averaged particle velocity *V* (in [10] pore averaged velocity was used).

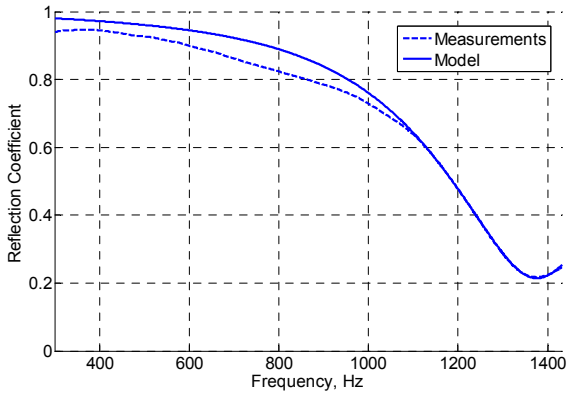

Fig. 2 Comparison between model, Eq.(4) to Eq.(7), predictions (solid line) and data (dashed line) for the reflection coefficient. Hard backed layer of lead shot, thickness of 0.04 m.
Parameters of the material are given in Tab. 1.

Looking at a single convolution integral that appears in both equations, we can write:

$$I_c(t) = \int_{-\infty}^{t}\frac{1}{\sqrt{\pi\tau(t-t')}}\exp\left(-\frac{t-t'}{\tau}\right)g(t')dt' \tag{10}$$

where $g(t)$ is one of the field variables $\partial_x P$ or $\partial_t P$. For a numerical implementation, the field variable is calculated at discrete time steps and therefore the integration must be formulated as a discrete summation. It would be consistent with the finite-difference approximations to assume that the acoustic field variables vary only a little over each time step Δt. So, using the simplest assumption that $g(t)$ is constant over each time step, it is possible to say that

$$g(t) \simeq \sum_n \delta\left[\frac{t-(n-1)\Delta t}{\Delta t}\right]g(t_n) \tag{11}$$

where $t = n\Delta t$ and $\delta(x)$ is 1 for $0 < x \le 1$ and 0 elsewhere. Substituting Eq.(11) into Eq.(10), the convolution integral becomes

$$I_c(t_n) = \sum_{m=-\infty}^{n} g(t_m)\int_{t_{m-1}}^{t_m}\frac{1}{\sqrt{\pi\tau(t_n-t')}}\exp\left(-\frac{t_n-t'}{\tau}\right)dt' \tag{12}$$

Replacing the variable t' by $z = \sqrt{\frac{t_n-t'}{\tau}}$ and decomposing the integral in two parts the following expression can be obtained

$$I_c(t_n) = \sum_{m=-\infty}^{n} g(t_m) \frac{2}{\sqrt{\pi}} \left[\int_0^{\sqrt{\frac{t_n - t_m}{\tau}}} \exp(-z^2) dz + \right. \\ \left. - \int_0^{\sqrt{\frac{t_n - t_{m-1}}{\tau}}} \exp(-z^2) dz \right] \quad (13)$$

where two Gaussian integrals are easily recognizable and are equal to $\frac{\sqrt{\pi}}{2} erf\left(\sqrt{\frac{t_n - t_m}{\tau}}\right)$ and $\frac{\sqrt{\pi}}{2} erf\left(\sqrt{\frac{t_n - t_{m-1}}{\tau}}\right)$ respectively. Finally we can say that the generic convolution integral is given by

$$I_c(n\Delta t) = \sum_{m=-\infty}^{n} g(m\Delta t) \left[erf\left(\sqrt{\frac{(n-m)\Delta t}{\tau}}\right) + \right. \\ \left. - erf\left(\sqrt{\frac{(n-m-1)\Delta t}{\tau}}\right) \right] \quad (14)$$

This approximation accurately converges to the solution if the stored past values of $g(t)$, used to convolve with the *erf*-function, corresponds to a past time that is larger than τ [5]. The FDTD scheme used in the present work is based on a spatial grid in which the velocity is offset from the pressure by one-half grid interval. This kind of scheme is known as staggered spatial scheme, the one-dimensional case of which is illustrated in Fig. 3.
The stability condition (Courant stability condition) of this scheme is given by

$$c \frac{\Delta t}{\Delta x} \ll 1 \quad (15)$$

where Δx is the spatial step and Δt is the time step. Because of the aliasing problem, it is suggested to use at least fifteen spatial steps per wavelength λ of the signal, [16], ($\lambda = c / f_c$, where f_c was the central frequency of the signal). It is also important to take into account that the above condition is not the only one to be satisfied for a good convolution integral approximation. It is imperative that the time step is much smaller than the smallest relaxation time used in the model.

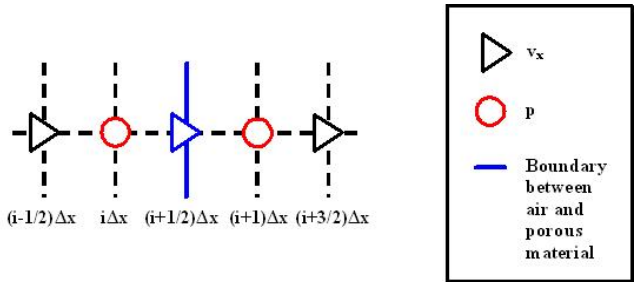

Fig.3 ,Spatially staggered finite difference scheme. The solid line is the boundary between the two regions: air and porous medium. Triangles are velocity nodes and circles are pressure nodes.

For the derivative approximations, a forward time and backward space approximation were implemented.

Following the scheme, one can see that the mass buoyancy *b* and the bulk modulus *K* must be stored at locations of pressure nodes. In air, the expressions used for the mass buoyancy and the bulk modulus are $b = \rho_0^{-1}$ and $K = \gamma P_0 = \rho_0 c_0^2$ whereas in the porous medium they are $b = \frac{\phi}{\rho_0 \alpha_\infty}$ and $K = \frac{\gamma P_0}{\phi}$. Others parameters that must be stored are the relaxation times τ_m and $\tau_{e,m}$. Because of the chosen scheme, the values of the mass buoyancy and viscous relaxation times need to be defined at the spatial nodes on the boundary between air and the porous medium. For the mass buoyancy, the averaged value between the mass buoyancy of air and porous medium was used. For the viscous relaxation times it was convenient to define a relaxation frequency $f_v = \frac{1}{\tau_v}$. Even though the viscous relaxation time in air is infinite, the relaxation frequency is zero, which allows calculations of the averaged relaxation frequency between air and porous medium.

Samples	Lead Shot	Marbles
Radius [m]	$1.55 \cdot 10^{-3}$	$7.70 \cdot 10^{-3}$
ϕ	0.36	0.40
α_∞	1.89	1.75
σ $[Pa \cdot s \cdot m^{-2}]$	$3.01 \cdot 10^{3}$	76.26
Λ $[m]$	$4.02 \cdot 10^{-4}$	$2.37 \cdot 10^{-3}$
M	1.57	1.48
τ_1 $[s]$	$1.50 \cdot 10^{-3}$	$5.09 \cdot 10^{-2}$
τ_2 $[s]$	$7.51 \cdot 10^{-3}$	$2.27 \cdot 10^{-1}$
Λ_e $[m]$	$5.62 \cdot 10^{-4}$	$3.42 \cdot 10^{-3}$
k' $[m^2]$	$1.60 \cdot 10^{-8}$	$6.02 \cdot 10^{-7}$
M'	1.12	1.03
τ_{e1} $[s]$	$2.04 \cdot 10^{-2}$	$7.10 \cdot 10^{-1}$
τ_{e2} $[s]$	$1.64 \cdot 10^{-3}$	$5.69 \cdot 10^{-2}$
τ^* $[s]$	$4.51 \cdot 10^{-3}$	$1.24 \cdot 10^{-1}$
τ_e^* $[s]$	$3.20 \cdot 10^{-3}$	$8.82 \cdot 10^{-2}$

Table 1 Samples and their characteristic parameters. Parameters with * are concerning to the Wilson *et al* model

4 Time domain measurements and comparisons with model predictions

The following experiment has been conducted in order to test the time domain model. The measurements set up is shown schematically in Fig. 4.
A theoretical "Mexican hat" pulse *f(t)* was used for the measurements:

$$f(t)=\left[1-(t-t_0)^2\,\omega_0{}^2\right]\exp\left[-\frac{(t-t_0)^2\,\omega_0{}^2}{2}\right] \quad (16)$$

The value of $\omega_0 = 3000$ rad/s was chosen to generate a pulse with duration of 3 milliseconds and central frequency equal to 675 Hz. The wavelength, which corresponds to this frequency, is much larger than the largest pore size in materials used thus allowing the use of the plane wave based model.

Using Matlab the function (16) was converted into a wave file, which was then uploaded into the B&K PULSE system and used as a source signal. The physical pulse was generated by the loudspeaker positioned at the bottom of the tube. The first microphone is located at a distance of 0.905 m from the loudspeaker and at 0.035 m from the surface of the sample. The sample holder is 0.10 m long and the second microphone is located at a distance of 0.017 m from the first one. The rigid termination at the end of the tube is 1.20 m far away from the second microphone.

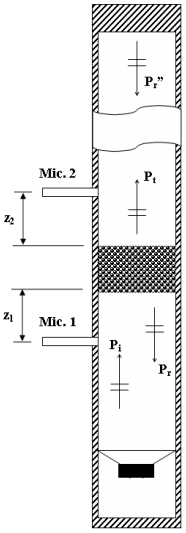

Fig. 4 Set up for time domain measurements.

Thanks to the combination of the pulse duration and the tube length, it was possible to distinguish clearly between the transmitted pulse and the one reflected by the rigid termination. Using the same set up, a series of measurements were taken. The first measurement, without the sample, was taken to record the signal generated by the loudspeaker (obviously different from the analytical one due to the loudspeaker response) in order to use in the numerical simulations. The other measurements were taken using different samples, where incident pulse, reflected pulse and finally the transmitted pulse were recorded in order to compare the data with numerical results.

Fixing the signal and varying the size of the spheres allowed investigations of the model performance in a range of pulse durations. According to the stability condition and the relaxation time values of the tested materials (Table 1), the following time and spatial steps were implemented in the code: $\Delta t = 2.03\mu s$ and, $\Delta x = 3.5mm$. The experimental set- up was reproduced in the numerical code. By storing the values of the pressure field at the nodes correspondent to the microphones positions, a comparison between these records and the data has been made. Furthermore, comparisons between the new model and the one used by Wilson *et al*. [5] have been performed.

For the model proposed in [5] the knowledge of only three parameters (porosity ϕ, flow resistivity σ and tortuosity α_∞) is required. The viscous and the thermal relaxation times are defined using the following equations

$$\tau = \frac{2\rho_0\alpha_\infty}{\sigma\phi} \quad (17)$$

$$\tau_e = N_{pr}s_B{}^2\tau \quad (18)$$

where s_B is a pore shape factor which is assumed to be equal to one here. Parameters for the new model are listed in Table 1. Two simulations were performed using marbles and lead shot. Results of these simulations are shown in Fig. 5 and Fig 6. As one can see good agreement between predictions of both models and the data was found. In the case of large spheres (marbles) the new model works better than the one proposed by Wilson *et al*., whereas for the smaller spheres the predictions of the two models are almost indistinguishable. For a quantitative comparison of both models, the averaged deviations of the predicted pressure values from the data points were evaluated for both transmitted and reflected pulses. For marbles, the new model deviations are around 3% and a 1% lower than those for the Wilson *et al*. model, for the transmitted and reflected pulse respectively.

In the case of lead shot, the agreement is better for the reflected pulse only, with 7.5% lower averaged deviation from measured data. For the transmitted pulse, [5] gives better agreement with the measurements due mostly to the slight time delay of the data with respect to the new model prediction.

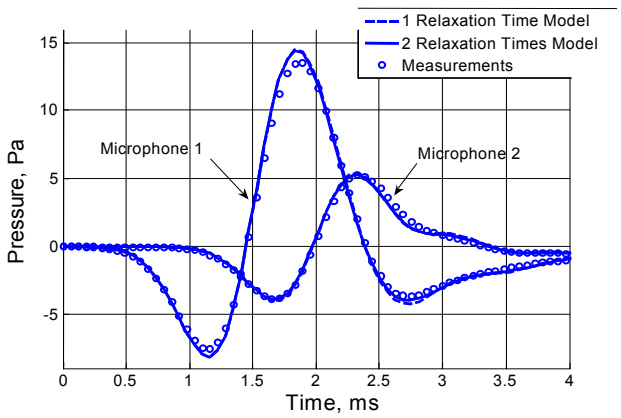

Fig. 6 Comparison between model predictions in time domain and measurements for a layer of marbles with thickness 0.1 m, other parameters are given in Tab. 1. Solid line – new model, dotted line – model [5], circles - recorded data.

The computational time required by the new model is about 20% longer compared to that needed by [5] as the number of convolution integrals has been doubled. This can be seen in Fig. 8 where relative difference $\frac{T_{2RT}-T_{1RT}}{T_{1RT}}$ between the time T_{1RT} required by [5] and the time T_{2RT} required by the new model is shown.

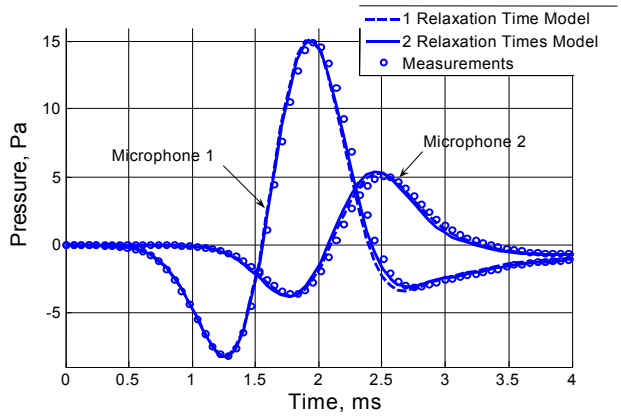

Fig. 7 Comparison between model predictions in time domain and measurements for a layer of lead shot with thickness 0.04m, other parameter are given in Tab. 1. Solid line- new model, dotted line – model [5], circles -recorded data.

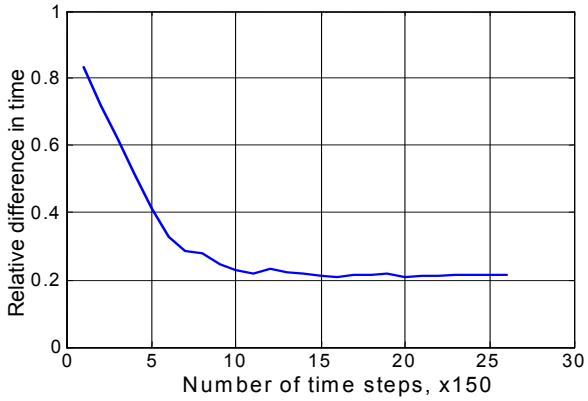

Fig. 8 Comparison of computational time required by the new model and model [5]. The required computational time was recorded every 150 time steps.

5 Conclusions

The new time domain semi-empirical model has been presented and numerically implemented in order to describe the acoustic behaviour of granular materials. It showed good agreement with the transmission and reflection measurements on packings of different size spheres. When compared to a simpler model described in [5], the new model is shown to require more computational time but to give a slightly improved agreement with the data for a larger size spheres. More measurements with different pulse durations are planned in the future in order to clearly demonstrate the advantages and the disadvantages of the new approach.

Acknowledgments

The project was supported by the EPSRC grant EP/E016529/1

References

[1] C.H. Lam, B.J. Kooij, A.T.D.Hoop, "Impulsive sound reflection from an absorptive and dispersive planar boundary", *J. Acoust. Soc. Am.* 116, 677-85 (2004)

[2] K Heutschi, M Horvath, J Hoffman, "Simulation of ground impedance in finite difference time domain calculations of outdoor sound propagation", *Acust. Acta Acust.* 91, 35-40 (2005)

[3] E.M. Salomons, R Blumrich, D Heimann , "Eulerian time-domain model for sound propagation over a finite-impedance ground surface. Comparison with frequency-domain models", *Acust. Acta Acust.* 88, 483-92 (2002)

[4] H Dong *et al*. "Sound propagation over layered poro-elastic ground using using a finite difference model", *J. Acoust. Soc. Am.* 108, 494-502 (2000)

[5] D.K. Wilson *et al.*, "Time-domain calculations of sound interactions with outdoor ground surfaces", *Appl. Acoust.* 68, 173-200 (2007)

[6] C Zwikker, C.W. Kosten, "Sound absorbing materials", *Elsevier, New York* (1949)

[7] K. Attenborough "Acoustical characteristic of rigid fibrous absorbents and granular materials", *J. Acoust. Soc. Am.* 73, 785-99 (1983)

[8] D.K. Wilson, V.E. Ostashev, S.L. Collier, "Time-domain equations for sound propagation in rigid frame porous media", *J. Acoust. Soc. Am.* 116, 1889-92 (2004)

[9] D.K. Wilson, "Simple, relaxational models for the acoustical properties of porous media", *Appl. Acoust.* 50, 171-8 (1997)

[10] D.L. Johnson, J. Koplik, R. Dashen, "Theory of dynamic permeability and tortuosity in fluid-saturated porous media", *J. Fluid. Mech.* 176, 379-402 (1987)

[11] O. Umnova, D. Turo, "Semi-empirical time domain model of sound attenuation in porous materials", *Acoustics'08 Paris.* (2008)

[12] BS EN ISO 10534-1, "Acoustics-Determination of sound absorption coefficient and impedance in impedance tube-Part 1: Method using standing wave ratio", (2001)

[13] BS EN ISO 10534-2, "Acoustics-Determination of sound absorption coefficient and impedance in impedance tube-Part 2: Transfer-function method", (2001)

[14] O. Umnova, K. Attenborough, K.M. Li, "Cell model calculations of dynamic drag parameters in packings of spheres", *J. Acoust. Soc. Am.* 107 (6), 3113-19 (2000)

[15] S. Gasser, F. Paun, Y. Bréchet, "Absorptive properties of rigid porous media: Application to face centered cubic sphere packing", *J. Acoust. Soc. Am.* 117 (4), 2090-9 (2005)

[16] J.P. Berenger, "A perfectly matched layer for the absorption of electromagnetic Waves", *J. Comp. Phys.* 114 , 185-200 (1994)